Analysis of Land Surface Temperature and NDVI Using Geo-Spatial Technique: A Case Study of Keti Bunder, Sindh, Pakistan

Zia Ur Rehman[*], Syed Jamil H. Kazmi, Farheen Khanum and Zuber Ali Samoon

Department of Geography, University of Karachi, Karachi-75270, Pakistan

Abstract: Keti Bunder is a small coastal community situated at about 200 km south east of Karachi. It has four major creeks namely Chann, Hajamro, Kangri (Turchhan) and Khober with an arid subtropical climate and temperature remaining moderate throughout the year. This paper reports the application of an integration of Remote Sensing (RS) and Geographic Information Systems (GIS) for analysis and monitoring of the relationship of land surface temperature (LST) with Normalized Difference Vegetation Index (NDVI) in the area. LST is one of the critical elements in the natural phenomena of surface energy and water balance at local and global extent. [1-5]. Remote sensing in accord with tradition utilizes the NDVI to provide specific information on vegetation abundance to the LST–vegetation relationship. For mapping purposes, satellite images of Landsat-5 ETM+, Landsat-7 TM and Landsat-8 OLI / TIRS images, acquired on March 08, 2000, April 29, 2010 and April 08, 2014 respectively, were used. The results indicate that the maximum land surface temperature increased gradually from 39°C in 2000, to 42°C in 2010 and 45°C in 2014. Due to global warming and climatic changes. Keti Bunder of the Indus delta has experienced a serious condition over the past few years; the local communities have suffered badly from climate change impacts as heavy rainfalls, floods and cyclones have forced people to migrate to other places for their livelihood and shelter. However, mean NDVI value increased to -0.009 in 2014 as compared to 2010 (-0.165), due to several plantations of mangroves being established by the government. In the past, the mangrove forest was degraded due to lack of freshwater and seawater intrusion. The rate of degradation of mangrove forest in the delta was approximately 6 percent per year between 1980 and 1995 and only a small percentage of mangroves are now considered to be healthy [6-7].

Keywords: GIS, Remote Sensing, Land surface emissivity, vegetation abundance, Thermal Infrared, Atmospheric correction.

INTRODUCTION

In general, acquisition of data on land surface temperature (LST) consists of direct observation by using a network of local meteorological stations. These data have a high temporal resolution, but are expensive, poorly dispersed and difficult to convert into surface or raster efficient by using interpolation techniques. Remote Sensing Data are essentially cheaper to get and satellite data has been generally adopted by researchers with spatial reference in climatology because remote sensing data is available on a regular basis. Awareness of LST provides information on the temporal and spatial changes of the surface equilibrium state and is of basic importance in many applications [8]. The LST is used in many fields, including climate change, hydrological cycle, evapotranspiration, urban climate, vegetation monitoring, environmental studies and others [9-17]. Partly contested thermal infrared (TIR) data are commonly used to retrieve LST [17-18]. In recent years, thermal environmental studies have focused on the greenhouse effect and global warming; these use information on air temperature and LST [19].

LST provides a successful means of dividing lantern heat fluxes, and thus surface radiant temperature can be considered to be an expression of changing surface soil water content and vegetation cover [20]. This information supports inquiries into the relationship between LST and vegetation abundance [17, 21-23]. Various vegetation indices can be derived using remote sensing images, and regression analysis used to calculate percent vegetation cover. NDVI is used in semi-arid regions for vegetation production and soil moisture estimation. Normally vegetation has been monitored through different vegetation indices among which the NDVI is by far the most commonly used. However, NDVI has been shown to respond primarily in the high-absorption red affected band.

The Indus River has its source in Mansarover Lake in the Tibet Plateau (China). Its height above sea level is 5182 m. The length of the Indus River is 2900 km from the source down into the Arabian Sea. Before reaching the Arabian Sea, the Indus River travels on the extensive Indus plain through a delta close to the border of India, known as the 'Indus Delta'. Keti Bunder's climate is typical of South Asian coastal areas. January is the coolest month with a minimum temperature of 9.5°C, while in June and July temperatures range from 23°C to 36°C [24]. Mild winters come from November to February while summer season remains from March to October.

*Address correspondence to this author at the Department of Geography, University of Karachi, Karachi-75270, Pakistan; Tel: +92(0)20-9926-1300-7, Ext. 2452/3292; Fax: 92-21-9924-3206; E-mail: zia_rockies@yahoo.com

Average annual rainfall is 220 mm and occurs mainly during the monsoon season. During last century Keti Bunder changed location three times due to seawater intrusion. Resources such as surface freshwater and underground water have been degraded due to sea water intrusion into Keti Bunder. The Indus Delta is listed under the Ramser Convention on Wetlands 1971 and is classified as the 5th largest delta of the World [25]. The Indus Delta consists of 17 major and numerous minor creeks, which are now full of sea water; presently freshwater is receiving only between the area of Hajamro and Kharak Creeks (Shah Bunder Taluka) through one main outlet to the sea, Khobar creek. In the past, people used to grow red rice, banana, coconut and melons. The fertile land has been destroyed by waterlogging and salinity. Similarly, eight species of mangroves formerly occurred in the area. Now, the only three are *Avicenna marina*, *Aegiceras corniculata* and *Rhizophora mucronata*. Mangrove growth has seriously declined, owing to the decrease of fresh water [26].

Study Area

The study area is located from Dabbo Creek to Khobar Creek, almost the entire area of Keti Bunder (Figure **1**). It lies approximately between latitude 24° 22' 0" N to 23° 55' 0" N and longitude 67° 15' 30" E to 67° 35' 0" E. It is located around 200 km south-east from the city of Karachi and Sindh Province. Once, Keti Bunder was the prosperous commercial centre of the delta, which is the gateway to the Arabian Sea. The Keti Bunder is surrounded by a rip-rap (sloped stone facing) seawall (about 2-meters above the high water mark), and the town, which is isolated in the mudflats on Hajamro Creek (which used to be connected to a branch of the Indus River), is connected to "dry" land by a two-lane road, which is protected by rip-rap, but at low elevation about 1-1.5 metres above the high water mark [27]. The Union Council of Keti Bunder comprises 42 settlements out of which 28 have already been engulfed by seawater [28]. The main source of livelihood is marine fishing.

Objectives of the Study

➢ To perform a temporal analysis of LST and NDVI using Landsat satellite imageries in the study area.

➢ To examine the relationship between LST and NDVI over time.

METHODOLOGY

1) Data Acquisition

Two main sources of data collection were used to obtain primary and secondary data. The most important data in this study were the satellite data. Other data were collected from governmental and non-governmental organizations and published materials.
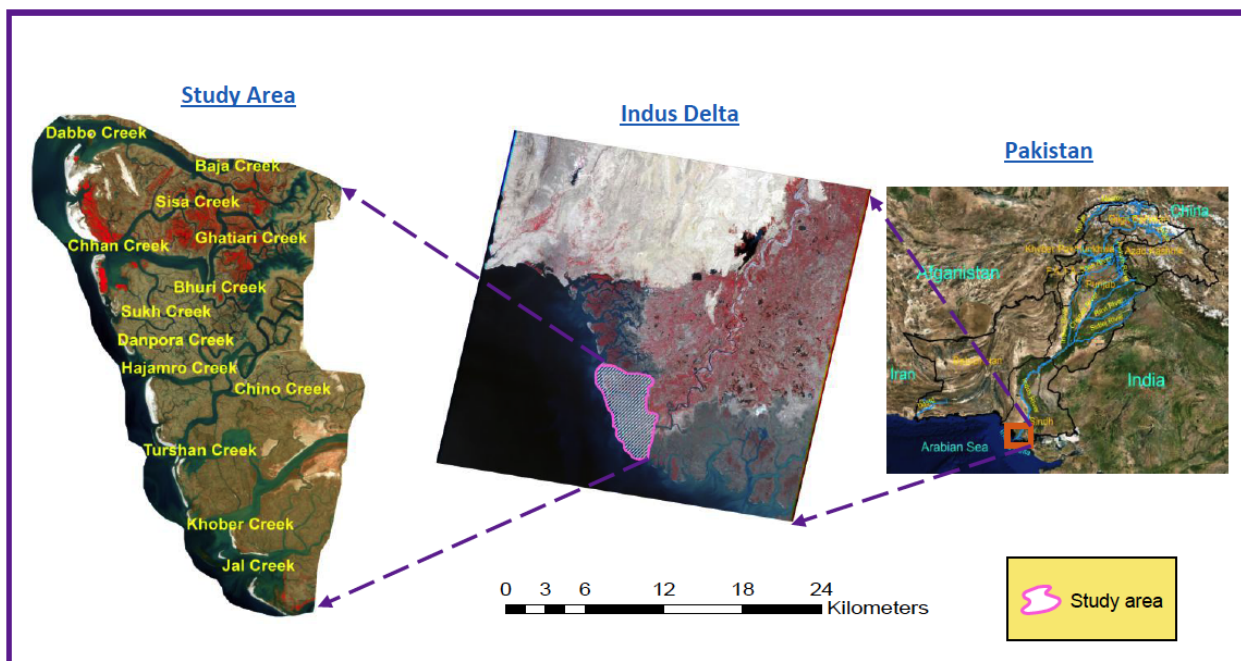

Figure 1: Location map of the study area.

Table 1: Details of Landsat Data Collected

S. No.	Date of Images	Satellite	Sensors	Resolution (m)	Bands	Thermal Band
1.	08-04-2014	LANDSAT-8	OLI / TIRS	30	11	10, 11
2.	29-04-2010	LANDSAT-5	TM	30	7	6
3.	08-03-2000	LANDSAT-7	ETM+	30	7	6

i. Satellite Data

Satellite data were utilized in this study. This data has been freely downloaded from official Earth Explorer USGS distribution website (earthexplorer.usgs.gov). All the satellite data were referenced to the Universal Transverse Mercator (UTM) Projection System and depended of one scene from the Worldwide Reference System (WRS-2) of path 152 and row 043. The details are given in Table **1**.

ii. Published Data

The published research work of different relevant articles was used to provide guidance for this study.

2) Software

After the collection of data, RS and GIS software were used for the analysis and further processing. These are ERDAS Imagine 2013 and ArcGIS 10.1.

3) RS &GIS Techniques

i. Atmospheric Correction

Cloud cover affects not only the ability to sense what is beneath the clouds using certain bands, but can also increase the Digital Number (DN) values of adjacent pixels. Clouds scatter light, thereby increasing brightness measured from ground features. Shorter wavelengths, such as TM 5 bands 1, 2, and 3 (blue, green, and red) scatter more than longer wavelengths [29-31]. Consequently, adjacent pixels can be affected because clouds often have gradations of vapour, moisture leading to the cloud centre. Additionally, cloud shadow may be cast further from the adjacent pixels, thereby darkening the brightness component other pixels. Recommended dark object correction for LST, NDVI, classification and change detection application involves a two-step procedure of atmospheric correction.

➤ First, the raw image is radiometrically corrected by converting the DN values to at-sensor radiance.

➤ In the second step, the image is atmospherically corrected by calculating spectral reflectance with the use of the spectral radiance ascertained in the first step.

ii. Land Surface Temperature

Land surface temperature (LST) is the main factor used to determine energy exchange and surface radiation [32]. Nowadays, one of the most widely used methods to retrieve LST is to employ thermal infrared (TIR) -remote sensing data. The following equations are provided by the Landsat User's Handbook [33].

$$\text{Radiance} = \frac{\text{LMAX} - \text{LMIN}}{\text{QCALMAX} - \text{QCALMIN}} \times (\text{QCAL} - \text{QCALMIN}) + \text{LMIN} \quad (1)$$

Where,

LMAX = the spectral radiance that is scaled to QCALMAX in W/ (m^2 * sr * μm)

LMIN = the spectral radiance that is scaled to QCALMIN in W/ (m^2 * sr * μm)

QCALMIN = the minimum quantized calibrated pixel value (corresponding to LMIN) in DN = 1,

QCALMAX = the maximum quantized calibrated pixel value (corresponding to LMIN) in DN=255 (TM / ETM+),

QCALMAX = 65535 (landsat-8 OLI / TIRS)

QCAL = DN

Firstly brightness temperature, NDVI, and emissivity were calculated from TM, ETM+ and OLI / TIRS images, which were then used to compute LST, while the DN value of Landsat-8 OLI / TIRS image is 65535.

TB = K2/Log {(K1/Radiance) +1)} (2)

Where,

TB = the effective at-satellite brightness temperature in Kelvin;

K1 = 666.09 (watts/ (meter2 × ster × μm))

K2 = 1282.71 (Kelvin) are calibration constants; and

Final LST is estimated by the following equation (3):

Land Surface Temperature= TB / {1+ (λ *BT/ρ*$log\varepsilon$)}   (3)

TB = Brightness Temperature

λ = Wavelength of emitted radiance (11.5 μm)

ρ = h x c/σ =1.438 x 10-2mK (σ=Boltzmann constant=1.38 x 10-23J/K,

h = Planck's constant=6.626 x 10-34Js, c=velocity of light=2.998 x 108m/s)

ε = Land surface emissivity

All calculations were performed at pixel level, and models established in ERDAS Imagine 2013.

iii. Normalized Difference Vegetation Index (NDVI)

Normalized Difference Vegetation Index (NDVI) is used as an indicator of biomass and greenness [34-36]. It is used as a standard for comparing vegetation greenness between satellite images [37-38]. The value ranges from +1 to -1, in which a positive value indicates a vegetated area and a negative value indicates a non-vegetated area. The following equation is used. (4).

$$NDVI = \frac{Near\,IR\,band - Red\,band}{Near\,IR\,band + Red\,Band}$$ (4)

iv. Pixel-by-Pixel Relationship between LST & NDVI

To examine the relationship between NDVI and LST, approximately 190 random point locations were taken for each LST and NDVI image by using 'Extract Multi values to point' tool in ArcGIS (Figure **2**).

1) Data Representations

The final data analysis is shown in the form of layouts, tables and graphs.

RESULT & DISCUSSION

1. Atmospheric Correction

The radiance measured through the sensors is affected by, and depends on, the existing atmospheric state at the time of taking the satellite image. Therefore, it is necessary to consider atmospheric conditions and to apply the required atmospheric correction. Before atmospheric correction, the NDVI statistic was in the range of -0.64486 to 0.2 for Landsat-7 ETM+, dated 08-03-2000. After applying of atmospheric correction, the range of NDVI was shifted to-0.46041 to 0.5821as depicted in Table **2**. Figure **3** depicts the NDVI image of the Landsat data before and after atmospheric correction. The image clearly
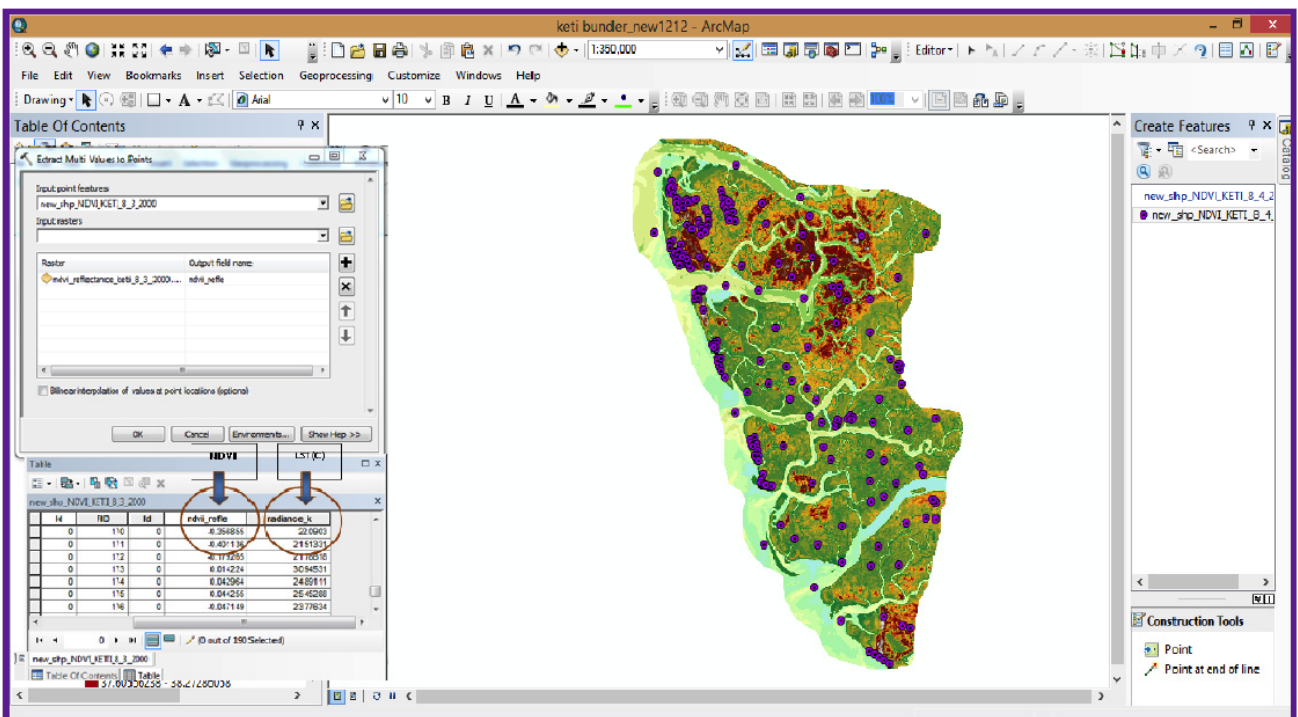

Figure 2: Print preview of Extract Multiple values to points in point shape files.

Table 2:   **Comparison between the NDVI Values of before and after Atmospheric Correction of Landsat-7 ETM+, Dated 08-03-2000**

S. No.	NDVI	NDVI before atmospheric correction	NDVI After atmospheric correction
1	Minimum	-0.64486	-0.46041
2	Maximum	0.2	0.5826
3	Mean	-0.426	-0.0084
4	Standard Deviation	0.122	0.184
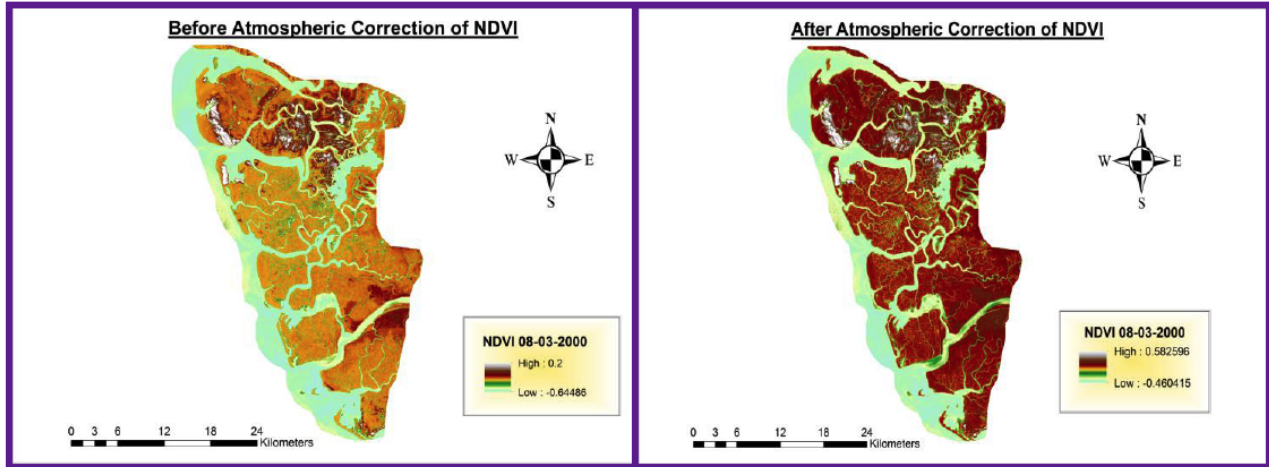
Figure 3: Comparison of NDVI maps before and after atmospheric correction of Landsat-7 ETM+, dated 08-03-2000.

indicates that the overall range of NDVI has been enhanced. Atmospheric correction was also performed on the images from Landsat-7 ETM+, dated 08-03-2000, Landsat-5 TM, dated 29-04-2010 and Landsat-8 OLI / TIRS, dated 08-04-2014, before deriving NDVI and LST.

2. Analysis of Land Surface Temperature

Land surface temperature images were acquired by developing a model in ERDAS Imagine 2013. LST images and results were as follows.

i. Analysis of LST of Landsat-7 ETM+, Dated 08-03-2000

Figure **4** shows the spatial distribution of surface temperature of Landsat-7 ETM+, on the date of 08-03-2000. LST ranged from 20°C to 39°C with a mean of 29.5°C. It can be observed from the image that north-west & south-eastern parts exhibit high temperature (30 °C to 39 °C), mainly due to land / bare soil and fallow land. Some of the temperature zones (26 °C to 30 °C) are also in mostly in north-eastern and southern parts of the image mainly due to dry mudflats. Some of temperature zones (30°C to 32°C) are mainly

mangroves. Some of the temperature ranges (28°C to 30°C) are existing wet mudflats and wet soil. The lowest temperature ranges (27°C to 28°C) occur in water bodies.

ii. Analysis of LST Landsat-5 TM, Dated on 29-04-2010

Figure **5** shows the spatial distribution of surface temperature of Landsat-5 TM, on the date of 29-04-2010. The LST ranged from 27°C to 42°C with a mean of 34.5 °C. The west and north-west parts exhibit high temperature (36°C to 42°C), mainly due to land / bare soil and fallow land near edge of creeks. Some of the temperature zones (32°C to 36°C) are also mostly in north eastern and southern parts of the image mainly due to dry mudflats. Some of temperature zones (30°C to 32°C) are mainly mangroves. Some of the temperature ranges (28°C to 30°C) are existing wet mudflats and wet soil. Lowest temperature ranges (27°C to 28°C) occur in water bodies.

iii. Analysis of LST of Landsat-8 OLI / TIRS, Dated 08-04-2014

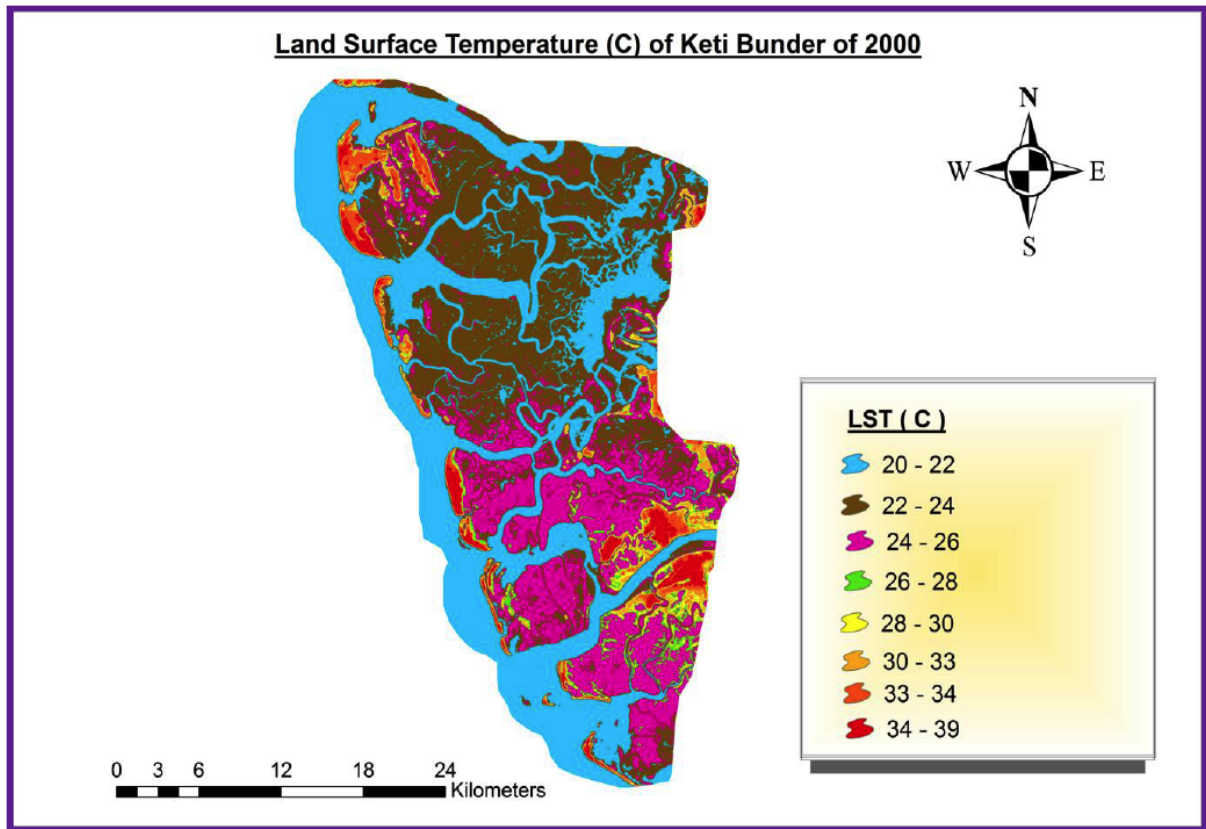Figure **6** shows the spatial distribution of LST of Landsat-8 OLI / TIRS, on the date of 08-04-2014.

Figure 4: Analysis of spatial distribution of land surface temperature (°C) of Landsat-7 ETM+, dated 08-03-2000.
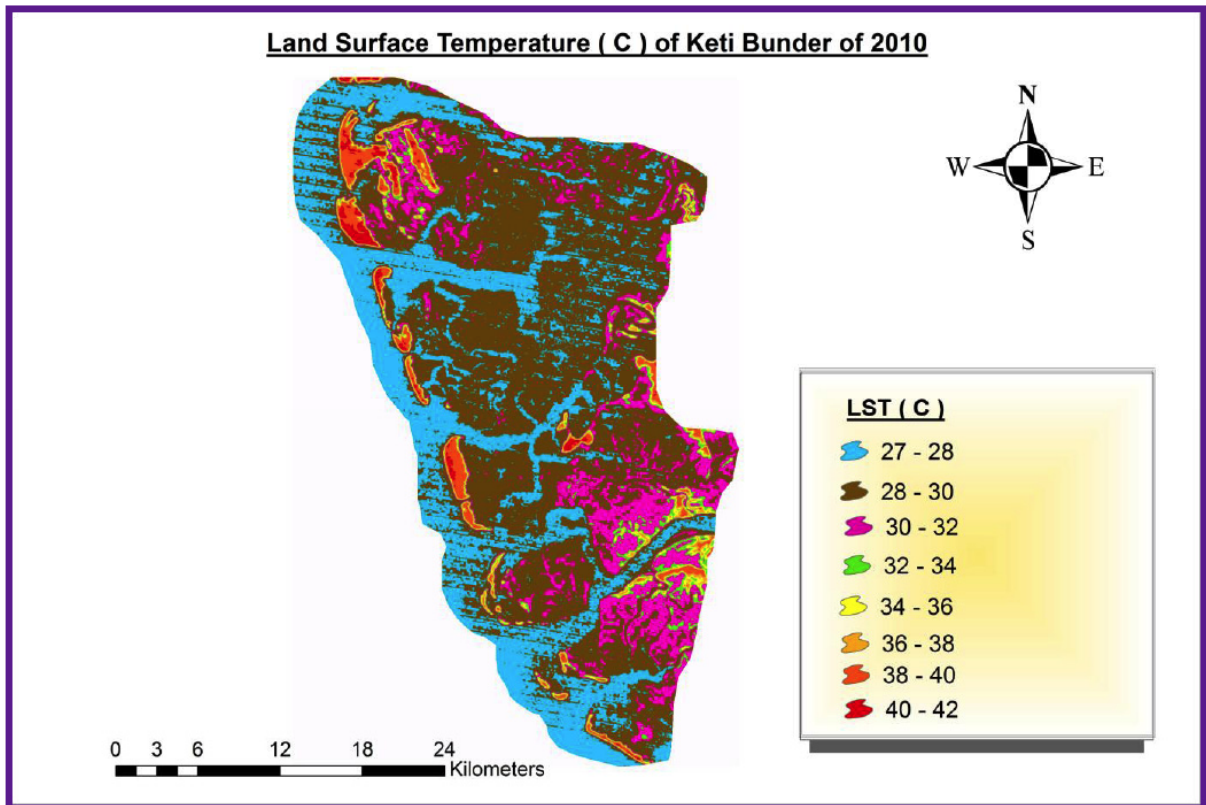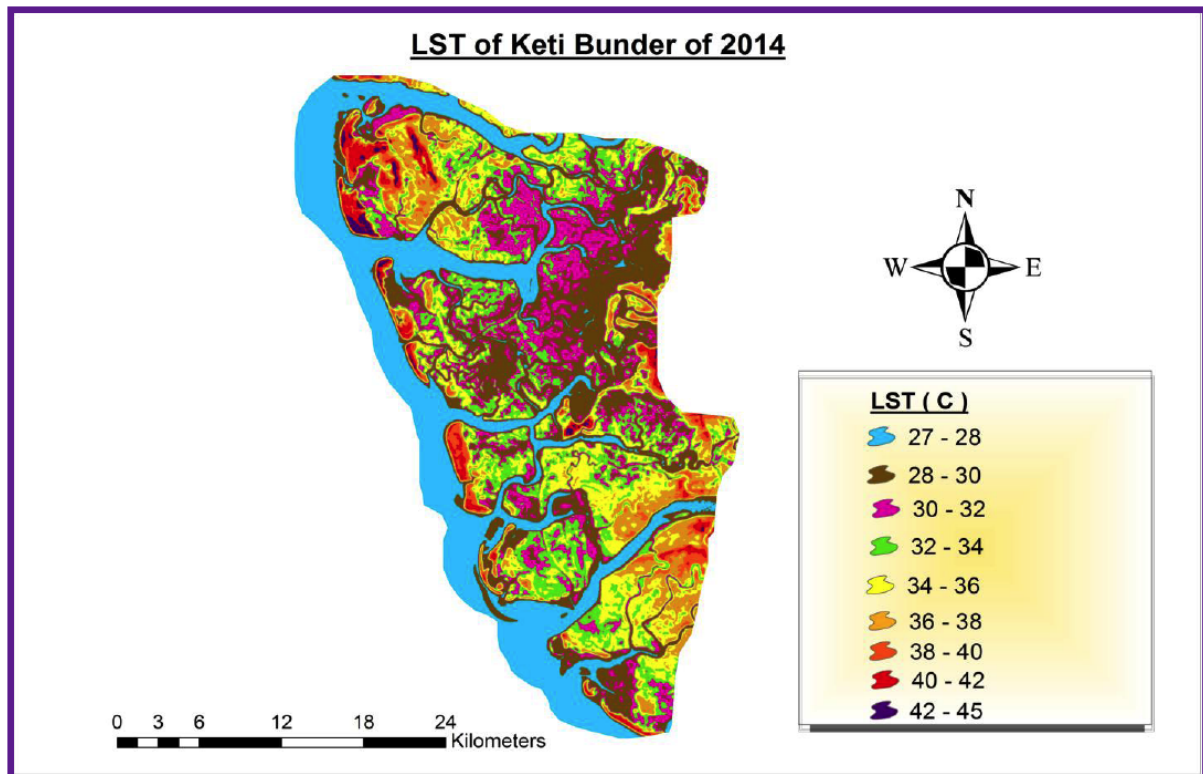

Figure 5: Analysis of spatial distribution of land surface temperature (°C) of Landsat-5 TM, dated 29-04-2010.

Figure 6: Analysis of spatial distribution of land surface temperature (°C) of Landsat-8 OLI / TIRS, dated 08-04-2014.

The LST ranged from 27°C to 45°C with a mean of 36°C. The west, north-west & south-west parts exhibit high temperature (36°C to 45°C), mainly due to land / bare soil and fallow land near the edge of creeks. Some of the temperature zones (32°C to 36°C) are also mostly in the southern part of the image mainly due to dry mudflats. Some of temperature zones (30°C to 32°C) are mangroves. Some of the temperature ranges (28 °C to 30 °C) are existing wet mudflats. Lowest temperature ranges (27 °C to 28 °C) occur in water bodies.

iv. Comparative Discussion of Analysis of Land Surface Temperature (LST)

Figures **4**, **5** & **6** show that the surface temperature of Keti Bunder was increasing continuously. The maximum temperature was 39°C in 2000, 42°C in 2010 and 45°C in 2014. The temperature rise was 3°C in the period 2000 - 2010 (i.e. 10 years) and also 3°C in the period 2010 - 2014 (just 4 years). The analysis shows a very rapid rise in temperature of Keti Bunder and its surrounding areas.

During the 20th century, the increase in the global temperature was recorded as 0.76 °C [39]. It is expected that temperatures will increase further between 1.4°C and 5.8°C by 2100 and the rise of temperature will continue long after that [40-41]. Keti

Bunder is vulnerable due to cyclones and tsunamis. The intensity of cyclones has notably increased during last the 30 years, possibly owing to global warming. Thousands of Keti Bunder residents may be displaced in the coming few years due to the impacts of storms, rising sea levels, and other expected effects of climate change [24]. The climate projection indicates that at least a 5°C rise will occur in the Indus Delta by the end of the 21st century. The first two decades upto 2030 do not play or amusement any rise in temperature rather hard to move conditions are evidence. After there is a sharp go higher in temperature at a rate of 0.5 °C per 10 years stage until 2070 later it becomes least. Figure **7** shows future predicted baseline of temperature of Keti Bunder [42].

Sindh coast is at high risk of tropical cyclones due to climate change and rise of temperature. It is a huge threat to the land covers, human population and biodiversity. In the past, Sindh coastline was widely exposed to disasters like the flood, frequent storms, and cyclones. This coast faces cyclones approximately every year (Figure **8**) [43] and high tides shown in Figure **9**.

Major cyclones during the last 100 years, which hit the Sindh coast were in May 1902, June 1926, June 1964, November 1993, June 1998, May 1999
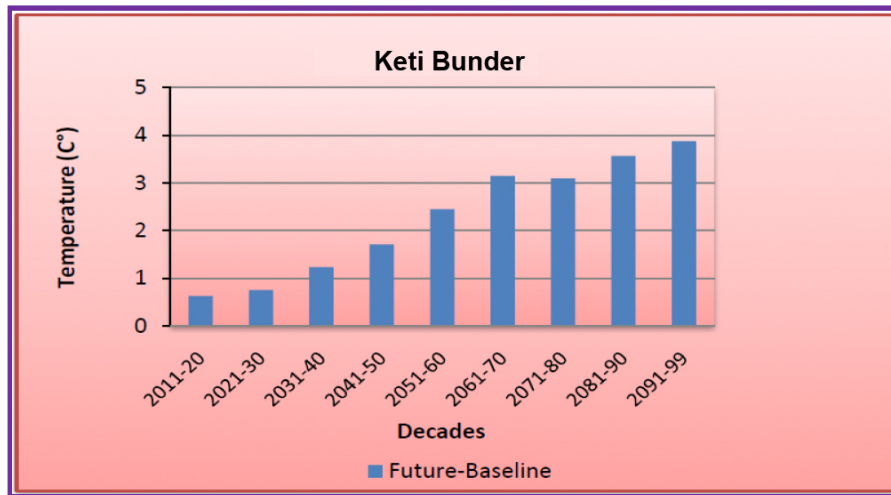
Figure 7: Future-baseline (2011 to 2099) of temperature of Keti Bunder. (Source: pmd.gov.pk).
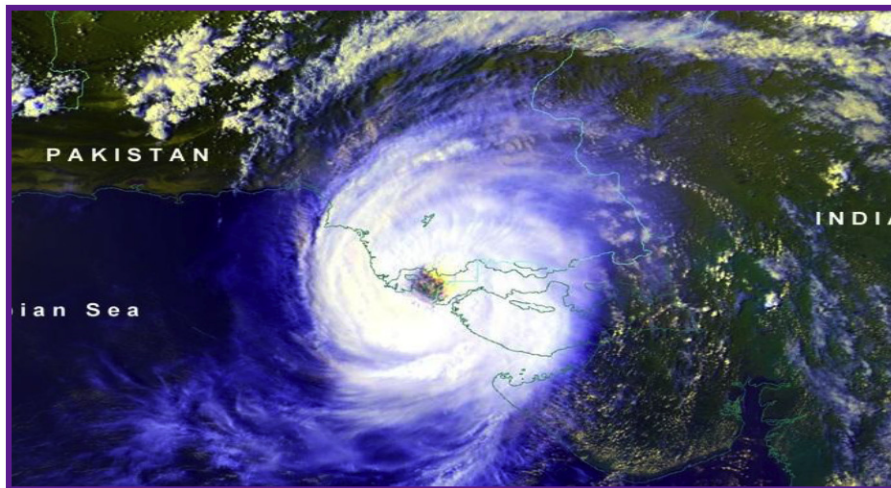

Figure 8: Cyclone in North Arabian Sea. (Source: Pakistan weather portal 2011).

Figure 9: High tides in Hajamro Creek. (Source: Author).

(Cyclone– 02A), 2004 (Cyclone Onil), June 2007 (Cyclone 'Gonu' and 'Yemyin'), 2010 (PHET), 2011 (KIELA) and 2014 (Nelofar). Cyclones 2007 (Yemyin) and 2010 (Phet) were the most dramatic and serious climatic disasters to have hit districts Thatta and Gwadar. The resulting human and environmental disasters, exacerbated due to poor planning and management, had consequences that the people of the
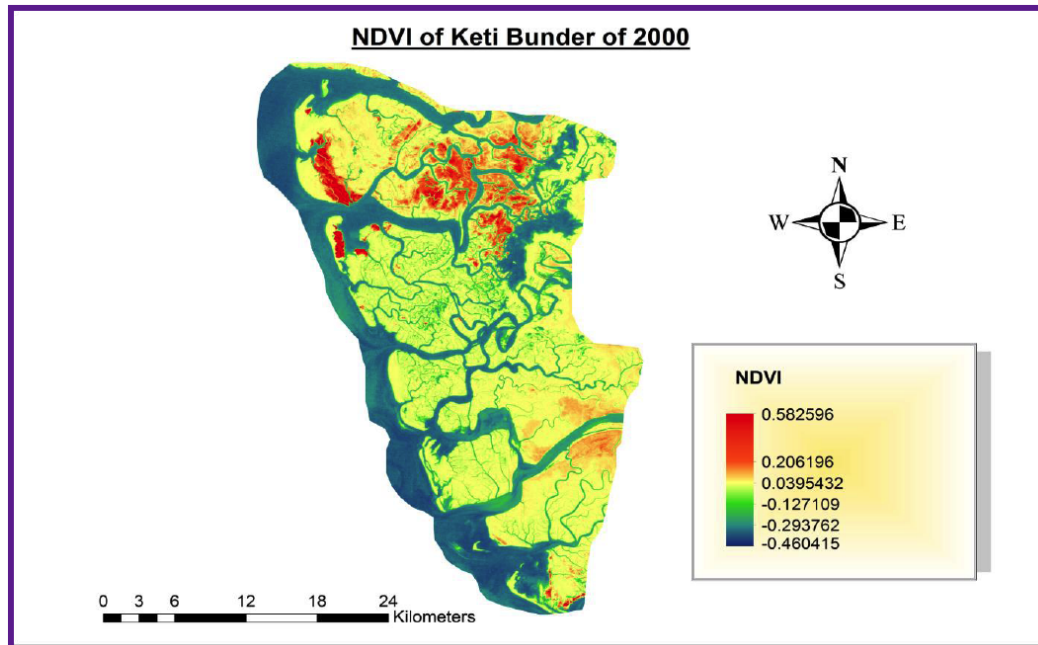
Figure 10: Analysis of spatial distribution of the Normalized Difference Vegetation Index (NDVI) of Landsat-7 ETM+, dated 08-03-2000.

Indus Delta and coastal Baluchistan are still recovering from.

3. Analysis of Normalized Difference Vegetation Index (NDVI)

NDVI is one of the most widely used indexes in satellite analysis and monitoring of vegetation cover area. NDVI images were obtained by ERDAS Imagine 2013. The final NDVI images and results are as follows.

i. Analysis of NDVI of Landsat-7 ETM+, Dated 08-03-2000

Figure **10** shows the spatial distribution of NDVI of Landsat-7 ETM+, dated 08-03-2000. The NDVI values are estimated range of -0.460415 to 0.582596, having a mean value of -0.084 and standard deviation of 0.184. Higher NDVI values 0.582596 and 0.206196 are observed over mangrove areas in the northern part of the image (red & orange areas). The other NDVI value of 0.0395432 shows mudflats in the image (yellow areas). The lowest NDVI values of -0.127109 to -0.460415 show water bodies (light green and blue areas).

ii. Analysis of NDVI of Landsat-5 TM, Dated on 29-04-2010

Figure **11** shows the spatial distribution of NDVI of Landsat-5 TM, dated 29-04-2010. The NDVI values are estimated range of -0.383238 to 0.514505, having a

mean value of -0.165 and standard deviation of 0.139. Higher NDVI values of 0.514505 to 0.334956 are observed over the mangrove area in the northern part of the image (red & orange areas). Other NDVI values of 0.155408 to -0.0241408 show mudflats in the image (light green and yellow areas). Some of the lowest NDVI values of -0.203689 to -0.383238 are observed over water bodies (blue areas).

iii. Analysis of NDVI of Landsat-8 OLI / TIRS, Dated 08-04-2014

Figure **12** shows the spatial distribution of NDVI of Landsat-8 OLI / TIRS, dated 08-04-2014. The NDVI values are estimated in the range of -0.191272 to 0.405551, having a mean value of -0.009 and standard deviation of 0.086. Higher NDVI values of 0.405551 to 0.28618 are observed over the mangrove area in the northern part of the image (red & orange areas). Other NDVI values of 0.166822 to 0.0474572 show mudflats in the image (yellow & very light green areas). Some of lowest NDVI values -0.0719074 to -0.191272 are observed over water bodies (light green, white & blue areas).

iv. Comparative Discussion of Analysis of Normalized Difference Vegetation Index (NDVI)

Figures **10**, **11** & **12** and Table **3** show that all positive values represent the mangrove area. In year 2000, the mean NDVI value was -0.0084, which became -0.165 in 2010. In 2014 the mean NDVI value
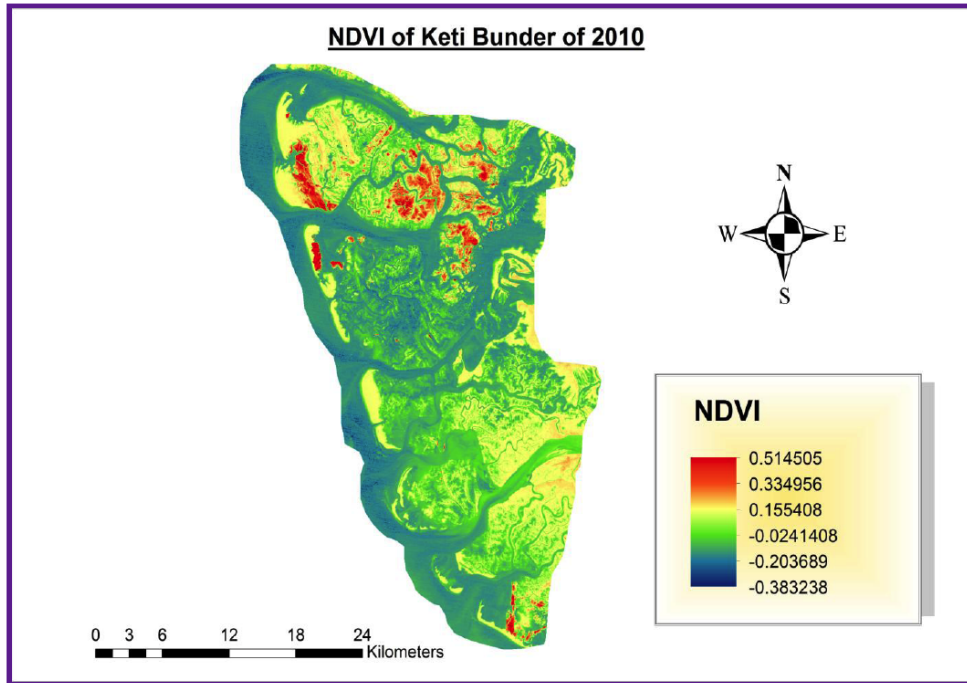
Figure 11: Analysis of spatial distribution of Normalized Difference Vegetation Index (NDVI) of Landsat-5 TM, dated 29-04-2010.
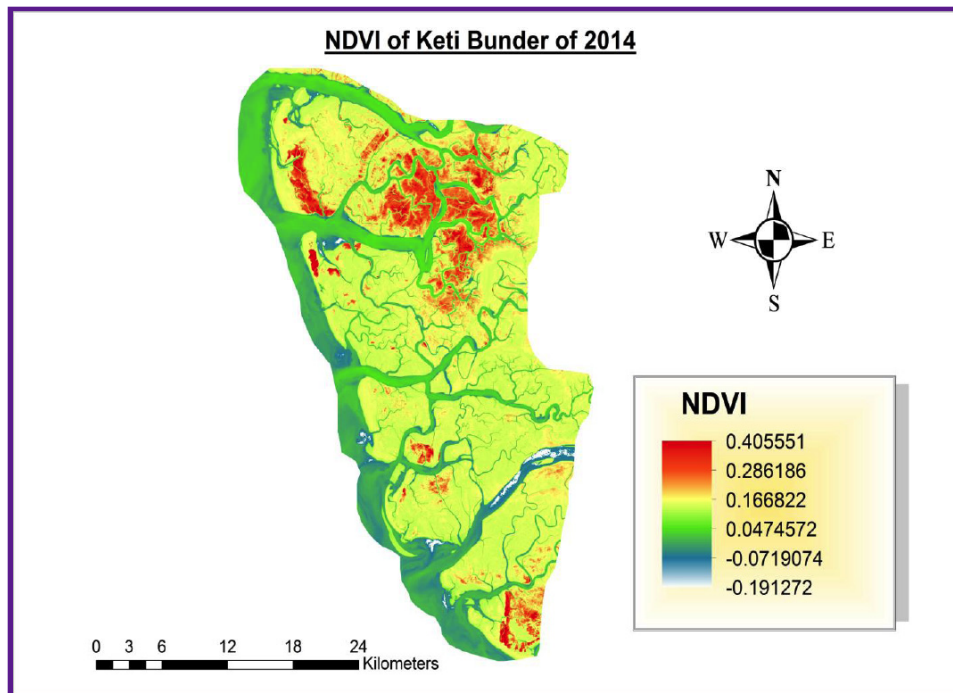

Figure 12: Analysis of spatial distribution of Normalized Difference Vegetation Index (NDVI) of Landsat-8 OLI / TIRS, dated 08-04-2014.

increased to -0.009. The reason is that several planning and plantation were made for mangroves in the area of Keti Bunder by organizations such as WWF and IUCN.

The key environmental resource in Keti Bunder is mangroves. The mangroves of Indus Delta represent the largest area of arid climate mangroves in the world. According to estimation, 95% of the mangrove area in the Indus Delta is composed of the species *Avicennia marina*. Relatively small patches of *Ceriops roxburghiana* (from the Rhizophora family) and *Aegicerias corniculata* (from the Myrinaceal family) are found near the mouth of the Indus at Keti Bunder [24].

Table 3:   NDVI Values of Different Years

S. No.	NDVI	NDVI of 08-03-2000	NDVI of 29-04-2010	NDVI of 08-04-2014
1	Minimum	-0.46041	-0.383238	-0.191272
2	Maximum	0.5826	0.514505	0.405551
3	Mean	-0.0084	-0.165	-0.009
4	Standard Deviation	0.184	0.139	0.086

Figure 13: *Rhizophora mucronata* and *Avicennia marina* mangroves plantation of Keti Bunder. (Source: Author).

Figure 14: Agriculture land swept by sea water or spoilt by water logging and salinity. (Source: Author).

Some plantation of mangroves in Figure **13**. Dense mangroves cover 2,631 hectares, medium mangroves cover about 1,996 hectares and sparse mangroves occupy 3,588 hectares [26]. Several hundred plants of *Rhizophora mucronata* mangroves were planted during the day-long operation on the these lands, where 451,176 mangrove saplings were planted on July 15, 2009 to make come into existence a record and win the Guinness Book of World Records gave respect to. The forest department now plans to plant at least 650,000 saplings within a day to break the record credited to India [44].

Around the Keti Bunder town, there is little vegetation cover. Water flow into the Indus Delta has declined from140 to 40 million acre feet (MAF) over the last few years and this, together sea level rise, has caused the increase of salinity of seawater and is detrimental to mangrove growth [25].

Red rice was formerly an agricultural commodity and was exported to other countries. The area was suitable for growing different kind of fruits, including coconuts, bananas and melons. Due to a reduction of freshwater flow, the sea has crept in and agricultural lands have either been swept by the sea water or spoilt by water logging and salinity (Figure **14**).

4. Pixel-by-Pixel Relationship between LST & NDVI

Approximately190 random points were selected from the LST and NDVI images and values acquired to
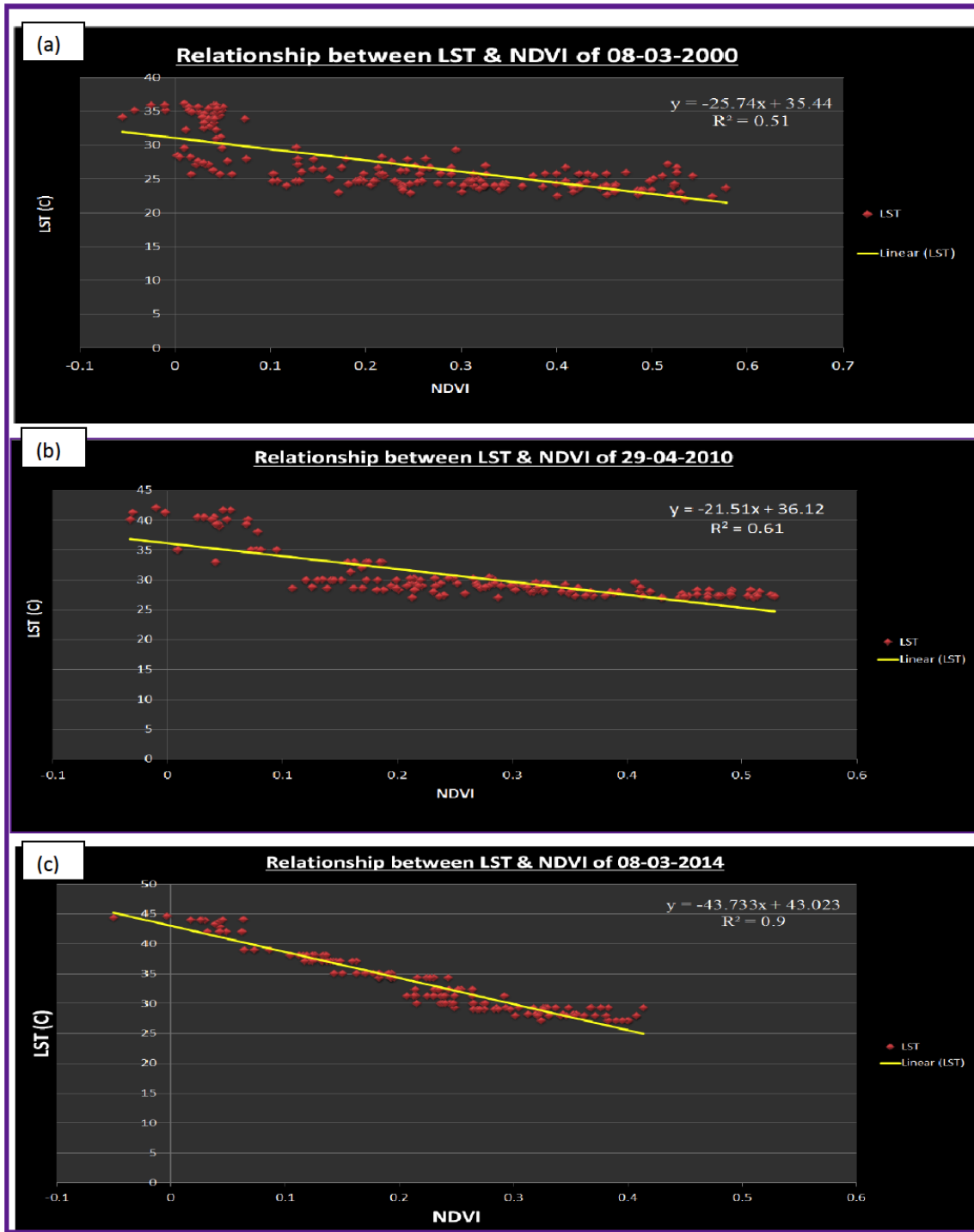
Figure 15: Linear regression of the relationships between LST and NDVI of study area; (**a**) 08-03-2000, (**b**) 29-04-2010 and (**c**) 08-04-2014.

find the correlation between LST and NDVI. Figure **15** indicates the correlation between LST and NDVI is 0.51 on 08-03-2000, 0.61 on 29-04-2010 and 0.91 on 08-04-2014. There is clear indication that the LST is strong, linearly and negatively correlated with NDVI in the year of 2014. However, there was a moderate and negative correlation in 2000 and 2010. Hence, areas with least vegetations are experiencing more LST.

CONCLUSION

It is concluded from the study that Geo-informatics techniques are very much helpful to evaluate, monitor and analyse the climate change effect on the coastal regions like Sindh Creeks, while it also provides a broad spectrum for the monitoring and mitigation regarding the climatic indicators. This area is prone to

the vulnerable cyclones. Therefore, these techniques are effective for the assessment of the major variables like vegetation and temperature. The Land Surface temperature in the study area is continuously increasing day by day, while the effect of temperature on Vegetation is quite noticeable especially in the creek area of Keti Bunder. The change in vegetation is not only due to the land degradation, but the increase in temperature is also affecting significantly on it. Whereas, the plantation of mangroves in the area is highly positive towards the nature. It would be worked as the barrier against the hazardous cyclones. The Geo-informatics techniques like LST and NDVI will be helpful to evaluate the present and future scenarios for the study area. It will be used as for the pre disaster management of coastal areas.

REFERENCES

[1]   Anderson MC, Norman JM, Kustas WP, Houborg R, Starks PJ, Agam N. A thermal-based remote sensing technique for routine mapping of land-surface carbon, water and energy fluxes from field to regional scales. Remote Sensing of Environment 2008; 112: 4227-4241.
http://dx.doi.org/10.1016/j.rse.2008.07.009

[2]   Brunsell NA, Gillies RR. Length scale analysis of surface energy fluxes derived from remote sensing. Journal of Hydrometeorology 2003; 4: 1212-1219.
http://dx.doi.org/10.1175/1525-7541(2003)004<1212:LSAOSE>2.0.CO;2

[3]   Karnieli A, Agam N, Pinker RT, Anderson M, Imhoff ML, Gutman GG. Use of NDVI and land surface temperature for drought assessment: Merits and limitations. Journal of Climate 2010; 23: 618-633.
http://dx.doi.org/10.1175/2009JCLI2900.1

[4]   Kustas W, Anderson M. Advances in thermal infrared remote sensing for land surface modelling. Agricultural and Forest Meteorology 2009; 149: 2071-2081.
http://dx.doi.org/10.1016/j.agrformet.2009.05.016

[5]   Zhang R, Tian J, Su H, Sun X, Chen S, Xia J. Two improvements of an operational two-layer model for terrestrial surface heat flux retrieval. Sensors 2008; 8: 6165-6187.
http://dx.doi.org/10.3390/s8106165

[6]   World Wildlife Fund - Pakistan. Keti Bunder Village Development Plan. WWF Regional Office Karachi 2005.

[7]   World Wildlife Fund - Pakistan. Study on Knowledge, Attitudes & Practices of Fisher folk Communities about Fisheries and Mangrove Resources - Keti Bunder 2005.

[8]   Kerr YH, Lagouarde JP, Nerry F, Ottlé C. Land surface temperature retrieval techniques and applications. In Quattrochi DA, Luvall JC, Eds. Thermal remote sensing in land surface processes 2000; (pp. 33-109). Boca Raton, Fla.: CRC Press.

[9]   Arnfield AJ. Two decades of urban climate research: a review of turbulence, exchanges of energy and water, and the urban heat island. International Journal of Climatology 2003; 23: 1-26.
http://dx.doi.org/10.1002/joc.859

[10] Bastiaanssen WGM, Menenti M, Feddes RA, Holtslag AAM. A remote sensing Surface Energy Balance Algorithm for Land (SEBAL). Formulation. Journal of Hydrology 1998; 212: 198-212.
http://dx.doi.org/10.1016/S0022-1694(98)00253-4

[11] Hansen J, Ruedy R, Sato M, Lo K. Global surface temperature change. Reviews of Geophysics 2010; 48: RG4004.
http://dx.doi.org/10.1029/2010RG000345

[12] Kalma JD, McVicar TR, McCabe MF. Estimating land surface evaporation: A review of methods using remotely sensed surface temperature data. Surveys in Geophysics 2008; 29: 421-469.
http://dx.doi.org/10.1007/s10712-008-9037-z

[13] Kogan FN. Operational space technology for global vegetation assessment. Bulletin of the American Meteorological Society 2001; 82: 1949-1964.
http://dx.doi.org/10.1175/1520-0477(2001)082<1949:OSTFGV>2.3.CO;2

[14] Su Z. The Surface Energy Balance System (SEBS) for estimation of turbulent heat fluxes Hydrology and Earth System Sciences 2002; 6: 85-100.
http://dx.doi.org/10.5194/hess-6-85-2002

[15] Voogt JA, Oke TR. Thermal remote sensing of urban climates. Remote Sensing of Environment 2003; 86: 370-384.
http://dx.doi.org/10.1016/S0034-4257(03)00079-8

[16] Weng Q. Thermal infrared remote sensing for urban climate and environmental studies: methods, applications, and trends. ISPRS Journal of Photogrammetry and Remote Sensing 2009; 64: 335-344.
http://dx.doi.org/10.1016/j.isprsjprs.2009.03.007

[17] Weng Q, Lu D, Schubring J. Estimation of land surface temperature, vegetation abundance relationship for urban heat island studies. Remote Sensing of Environment 2004; 89: 467-483.
http://dx.doi.org/10.1016/j.rse.2003.11.005

[18] Quattrochi DA, Luvall JC. Thermal infrared remote sensing for analysis of landscape ecological processes: Methods and applications. Landscape Ecol 1999; 14(6): 577-598.
http://dx.doi.org/10.1023/A:1008168910634

[19] Zhang J, Wang Y, Li Y. A C++ program for retrieving land surface temperature from the data of Landsat TM/ETM+ band6. Computers Geosci 2006; 32: 1796-1805.
http://dx.doi.org/10.1016/j.cageo.2006.05.001

[20] Owen TW, Carlson TN, Gillies RR. An assessment of satellite remotely sensed land cover parameters in quantitatively describing the climatic effect of urbanization. International Journal of Remote Sensing 1998; 19: 1663-1681.
http://dx.doi.org/10.1080/014311698215171

[21] Gallo KP, Owen TW. Assessment of urban heat island: a multisensory perspective for the Dallas-Ft. Worth, USA region. Geocarto International 1998a; 13: 35-41.
http://dx.doi.org/10.1080/10106049809354662

[22] Gallo KP, Owen TW. Satellite-based adjustments for the urban heat island temperature bias. Journal of Applied Meteorology 1998b; 38: 806-813.
http://dx.doi.org/10.1175/1520-0450(1999)038<0806:SBAFTU>2.0.CO;2

[23] Weng Q. A remote sensing-GIS evaluation of urban expansion and its impact on surface temperature in Zhujiang Delta, China. International Journal of Remote Sensing 2001; 22(10): 1999-2014.

[24] Gowdy JM, Salman A. Institution and Ecosystem Functions: The Case of Keti Bunder, Pakistan. Ecosystem Services Economic (ESE), Division of Environmental Policy Implementation, Paper N° 10. The United Nation Environment Program 2011.

[25] Abbasi AGN. Restoration of Singh's primary rights over River Indus. 18th convention of SANA, Cherry Hill; NJ 2002; 4-7.

[26] Glimpses. Indus for all programs, the journey a prosperous Indus ecoregion, WWF 2007-2008.

[27] CSF: a joint project of USAID and Pakistan Ministry of Finance. Analysis of Coastal Processes in the Indus Delta: Recent Trends, Future Projections, and Practical Interventions to Maintain Infrastructure, Services, and Livelihoods in the Delta 2010.

[28] Jensen JR. Introductory Digital Image Processing: A Remote Sensing Perspective. 2nd ed. Prentice Hall, Upper Saddle River, NJ 1996.

[29] Jensen JR. Introductory digital image processing; 3rd ed. Upper Saddle River, NJ: Prentice Hall 1996.

[30] Lillesand TM, Kiefer RW. Remote Sensing and Image Interpretation. 3rd ed. John Wiley & Sons, New York 1994.

[31] Song C, Woodcock CE, Seto KC, Lenney MP, Macomber SA. Classification and Change Detection Using Landsat TM Data: When and How to Correct Atmospheric Effects? Remote Sensing of Environment 2001; 75(2); 230-244.
http://dx.doi.org/10.1016/S0034-4257(00)00169-3

[32] Bobrinskaya M. Remote Sensing for Analysis of relationships between Land Cover and Land Surface Temperature in Ten Megacities. Master's of Science Thesis in Geoinformatics, TRITA-GIT EX 12-008, School of Architecture and the Built Environment, Royal Institute of Technology (KTH), Stockholm, Sweden 2012.

[33] National Aeronautics and Space Administration (NASA). Landsat Project Science Office: Landsat-7 Science data users hand book. Chapter: 11, Data Products 2004. (http.//www.gsfc.nasa.gov/IAS/handbook.htmls).

[34] Myneni RB, Dong JR, Tucker CJ, Kaufmann RK, Kauppi PE, Liski J, ZhouL, Alexeyev V, Hughes MK. A large carbon sink in the woody biomass of Northern Forests. Proceeding National Academy Sciences 2001; 98(26): 14784-14789.
http://dx.doi.org/10.1073/pnas.261555198

[35] Boone RB, Galvin KA. Generalizing El Nino effects upon Maasai livestock using hierarchical clusters of vegetation patterns. Photogrammetric Engineering and Remote Sensing 2000; 66(6): 737-744.

[36] Chen D, Brutsaert W. Satellite-sensed distribution and spatial patterns of vegetation parameters over a tall grass prairie. Journal of the Atmospheric Sciences 1998; 55(7): 1225-1238.
http://dx.doi.org/10.1175/1520-0469(1998)055<1225:SSDASP>2.0.CO;2

[37] Gillies RR, Carlson TN, Cui J, Kustas WP, Humes KS. A verification of the 'triangle' method for obtaining surface soil, water content and energy fluxes from remote measurements of the normalized difference vegetation index (NDVI) and surface radiant temperature. International Journal of Remote Sensing 1997; 18(15): 3145-3166.
http://dx.doi.org/10.1080/014311697217026

[38] Weng Q, Lo CP. Spatial analysis of urban growth impacts on vegetation greenness with Landsat TM data. Geocarto International 2001; 16(4): 17-25.
http://dx.doi.org/10.1080/10106040108542211

[39] Rasul G, Mahmood A, Sadiq A, Khan SI. Vulnerability of the Indus Delta to Climate Change in Pakistan. Pakistan Journal of Meteorology 2012; 8(16).

[40] Archer D. The Long Thaw. Princeton, NJ: Princeton University Press 2009.

[41] Intergovernmental Panel on Climate Change. Climate Change 2007: The Physical Science Basis. Contribution of working group I to the Fourth Assessment Report of the Intergovernmental Panel on Climate Change 2007, Geneva, Switzerland. Available at http://www.ipcc.ch

[42] Reference available from URL http://www.pmd.gov.pk/rnd/rndweb/rnd_new/climchange.php cited dated: 21 August 2014.

[43] Reference available from URL http://karachimetrological.files.wordpress.com/2011/03cyclone-karachi.jpg. Cited dated: 29 November 2014.

[44] Reference available from URL http://www.dawn.com/news/1013382/mangroves-plantation-near-keti-bunder-to-check-sea-intrusion cited dated: 30th May 2015.